Lab on a Chip

A floating 5-μm-diameter needle-electrode on the tissue for damage-reduced chronic neuronal recording in mice

Journal:	*Lab on a Chip*
Manuscript ID	LC-ART-11-2021-001031.R1
Article Type:	Paper
Date Submitted by the Author:	23-Dec-2021
Complete List of Authors:	Yamashita, Koji; Toyohashi University of Technology, Department of Electrical and Electronic Information Engineering Sawahata, Hirohito; National Institute of Technology Ibaraki College Yamagiwa, Shota; Toyohashi University of Technology, Department of Electrical and Electronic Information Engineering Yokoyama, Shohei; TechnoPro, Inc., TechnoPro R&D, Company Numano, Rika; Toyohashi University of Technology, Electoronics-Interdisciplinary Research Institute (EIIRIS); Toyohashi University of Technology, Department of Applied Chemistry and Life Science Koida, Kowa; Toyohashi University of Technology, Electoronics-Interdisciplinary Research Institute (EIIRIS); Toyohashi University of Technology, Department of Computer Science and Engineering Kawano, Takeshi; Toyohashi University of Technology, Department of Electrical and Electronic Information Engineering

ARTICLE

A floating 5-µm-diameter needle-electrode on the tissue for damage-reduced chronic neuronal recording in mice

Received 00th January 20xx,
Accepted 00th January 20xx

DOI: 10.1039/x0xx00000x

Koji Yamashita, [a] Hirohito Sawahata, [b] Shota Yamagiwa, [a] Shohei Yokoyama, [c] Rika Numano, [d,e] Kowa Koida, [d,f] and Takeshi Kawano *[a]

Microelectrode technology is essential in electrophysiology and has made contributions to neuroscience as well as to medical applications. However, it is necessary to minimize tissue damage associated with needle-like electrode into the brain tissue and the implantation surgery, which make the stable chronic recording impossible. Here, we report on an approach to use a 5-µm-diameter needle electrode, which enables the following of tissue motions by the surgical method. The electrode is placed on the brain tissue of the mouse with a dissolvable material while reducing the physical stress to the tissue; this is followed by implantation of the device in the brain without fixing it to the cranium while achieving a floating electrode on the tissue. The electrode shows the stable recording with no significant degradation of the signal-to-noise ratios for 6 months, and minimized tissue damage is confirmed compared to that when using the other cranium-fixed electrodes with the same needle geometry.

Introduction

Electrophysiology with microelectrode technology is an essential method in neuroscience, making contributions to the understanding of the nervous system and to medical applications. Extracellular signals with high spatiotemporal resolution can be recorded by penetrating a needle electrode into the tissue, such as multichannel-electrode array[1–4] or a flexible electrode to minimize mechanical mismatch between the needle (electrode) and the soft tissue of the tissue.[5–10] For long-term neuronal recording, it is necessary to minimize tissue responses, including neuronal death due to electrode penetration, and avoid the decrease in recording performance, including the signal-to-noise ratio (SNR) during device implantation. However, typical methods that employ these invasive needle electrodes with a diameter of more than 10 µm cause significant damage to brain tissue,[11–14] making stable recording impossible.[15,16]

Recent advances in microelectromechanical system technology enable us to fabricate extracellular needle electrodes with a diameter of less than 10-µm (e.g., <3 µm[17,18] for in vitro recording, 8.6 µm,[19] 5 µm,[20,21] 300 nm[22] for in vivo recording), thereby minimizing tissue response. In addition, in chronic applications, the physical stress at the interface between the device substrate [e.g., silicon (Si)] and tissue surfaces induces sustained inflammation and tissue response. In particular, the large geometry of the device substrate enhances areas of craniotomy and tissue damages. The approach reported in this study involves using an electrode device that has a 5-µm-diameter needle electrode on a 1 × 1 × 0.5 mm^3 substrate; in addition, a surgical procedure for the chronic device implantation is proposed. Because of brain tissue pulsation, conventional implantations, in which the electrode is fixed to the cranium, cause significant chronic inflammation[20] (Figure 1a1). To avoid these difficulties, a floating architecture for implantable devices, such as Smart dust on the tissue (nerve or muscle)[23,24] can be offered. By utilizing the surgical technique, the electrode device is implanted in the brain without being fixed to the cranium, resulting in a floating 5-µm-diameter needle electrode on the tissue to follow the pulsations (Figure 1a2). For physical stress reduction in the tissue during the electrode penetration, the device is attached to the manipulator with a material that dissolves. We demonstrated the device implantation in mice and chronic experiments while evaluating the signal quality and tissue damages.

Experimental

Microneedle-electrode device

[a] Department of Electrical and Electronic Information Engineering, Toyohashi University of Technology, Aichi, Japan
[b] National Institute of Technology, Ibaraki College, Ibaraki, Japan
[c] TechnoPro, Inc., TechnoPro R&D, Company, Tokyo, Japan
[d] Electronics-Interdisciplinary Research Institute (EIIRIS), Toyohashi University of Technology, Aichi, Japan
[e] Department of Applied Chemistry and Life Science, Toyohashi University of Technology, Aichi, Japan
[f] Department of Computer Science and Engineering, Toyohashi University of Technology, Aichi, Japan
*Corresponding author. E-mail: kawano@ee.tut.ac.jp.
Electronic Supplementary Information (ESI) available. See DOI: 10.1039/x0xx00000x

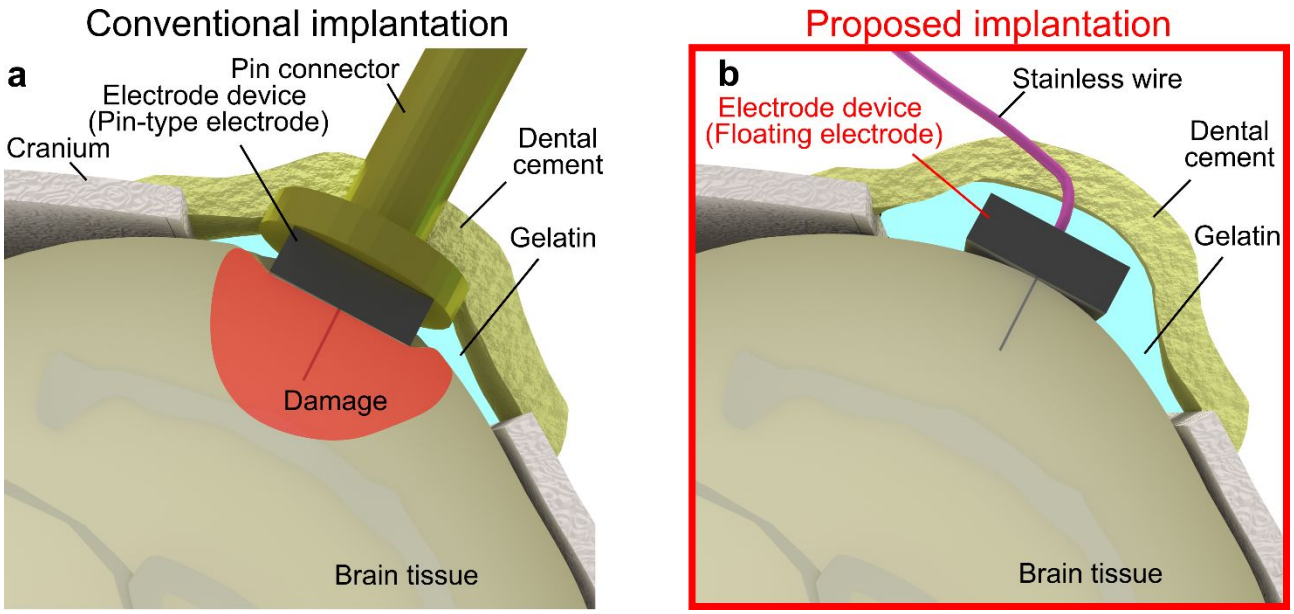

Figure 1. Comparison of electrode implantation. a) Schematic showing conventional implantation, in which the electrode is fixed to the cranium of the brain. b) Schematic showing the proposed implantation, in which the electrode packaged with a flexible lead is implanted in the brain without fixing to the cranium, achieving a "floating electrode" on the tissue.

We used a device that has a 5-µm-diameter and 400-µm-length microneedle electrode at the center of the 1 × 1 mm^2 Si substrate [n-type (111)-Si, resistivity = <0.02 Ω cm, thickness = 525 µm][20,25] (Figure 2a). We used a Si growth technology [gold (Au)-catalyzed vapor–liquid–solid growth of Si[26]] to fabricate the Si microneedle, which was then metalized with platinum (Pt) and titanium (Ti) (total Pt/Ti thickness = 200 nm) followed by the device encapsulation with a biocompatible insulator of parylene-C (1 µm in thickness, with the exception of the tip by plasma process).[20] To achieve the proposed floating electrode, the fabricated electrode device was packaged with an output lead of polyurethane-coated flexible stainless-steel wire (30 µm in diameter). For the device manipulation, the packaged electrode device in our prior work was mounted on a pin-type connector of Au using a paraffin wax, which plays a role in device detachment.[27] However, this material should be heated for melting (~70℃ for device detachment). To avoid the heating, we used polyethylene glycol (PEG) [two types of PEG with different melting characteristics were mixed, PEG 1000 : PEG 4000 = 1 : 1 (165-09085 for PEG 1000, 162-09115 for PEG 4000, FUJIFILM Wako Pure Chemical Corporation, Japan)], which dissolves in liquid (e.g., saline) at room temperature. Figures 2b-c show the device package with PEG paste. These two types of PEGs are spread on a dish and then heated (70℃), to mix as the liquid phase. The PEG paste is then applied to the tip of a pin connector, and the fabricated electrode device with the stainless wire is assembled. The PEG solidifies at room temperature and is ready for use in the animal experiment. Figure 2d illustrates an electrode device packaged with PEG paste and equipped with a stainless wire for the recording ["Pin connector (to recording system)" in Figure 2d]. Figure 2e shows SEM images of the overall and tip section of the fabricated microneedle electrode. The tip and bottom diameters of the microneedle were 1 and 10 µm, respectively.

Owing to the small geometry of the recording site of Pt, the microneedle electrode showed impedance magnitudes ranging from 290 ± 220 MΩ to 580 ± 38 kΩ at 10 Hz to 10 kHz [5.0 ± 0.8 MΩ (mean ± SD) at 1 kHz] in phosphate-buffered saline (PBS) at room temperature. To reduce the electrode impedance, the microneedle's tip was modified with a low impedance material of Pt black,[28] resulting in the impedance magnitudes that ranged from 6.3 ± 6.1 MΩ to 60 ± 12 kΩ [300 ± 150 kΩ (mean ± SD) at 1 kHz][20,21] (Figure 2f).

In vivo experiments

For the in vivo experiments, mice (wild - type C57 BL/6 mice, 20-30 g in weight) were anesthetized by isoflurane. After the head of a mouse was fixed with stereotaxic apparatus (SR-50, Narishige, Tokyo, Japan), parts of the cranium were removed [primary visual cortex (V1), 2.5 mm on the lateral side and 4.0 mm on the caudal side to the bregma, having a diameter of 1–3 mm]. The floating electrode device was attached to a micromanipulator (MO-10, Narishige) to control needle penetration as well as device placement. The recording site was stereotaxically defined, after which the microneedle penetrated the mouse's brain. After the device placement, the device was covered with a gelatin sponge, followed by being covered with dental cement. All experimental procedures were approved by the Committee for the Use of Animals at Toyohashi University of Technology, and all animal care followed the Standards Relation to the Care and Management of Experimental Animals (Notification No. 6, March 27, 1980 of the Prime Minister's Office of Japan).

In visual response recording, the mouse was sedated by intraperitoneal injection of chlorprothixene (100 µl of 0.5 % solution per 10 g body weight). For the visual stimulation to the

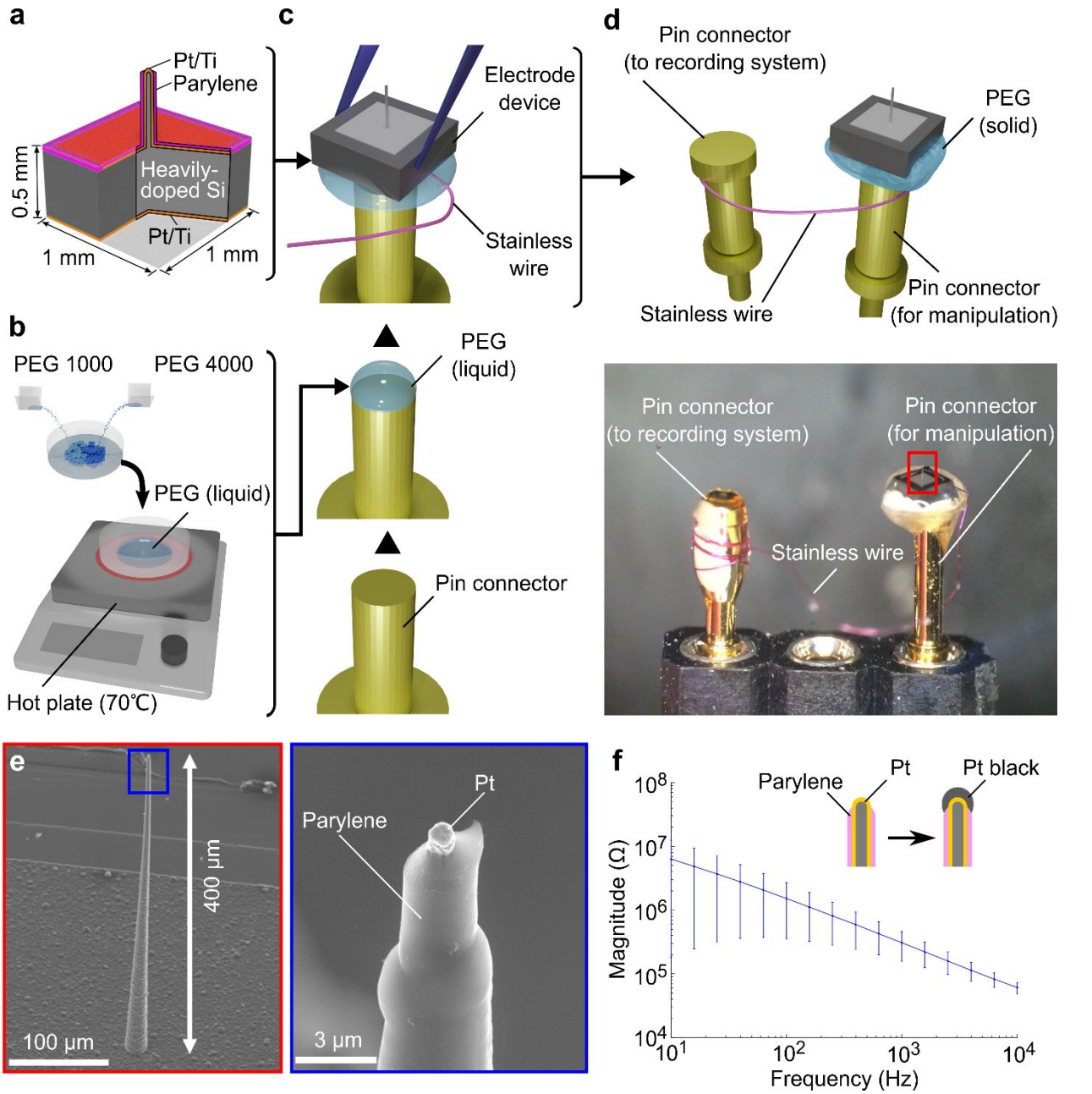

Figure 2. An electrode device. a) Schematic of the electrode device (1 × 1 mm^2 in surface area, 500 μm thickness), containing a needle electrode with a diameter of 5-μm and length of 400-μm in the center. b) PEG is prepared for the device package. c) Assembly of the electrode device on a pin connector via the PEG paste. d) Schematic and photograph of the packaged electrode device with an output lead (stainless-steel wire). e) SEM images of the overall needle and the needle tip portion. f) Impedance characteristics of Pt black plated microelectrodes measured at room temperature in PBS.

mouse, the mouse was illuminated with a white light-emitting diode (LED) in a dark room. The LED illuminated for 0.5 s at 3-s intervals was used. The LED was driven by a processing system (RZ2, Tucker-Davis Technologies, Alachua, USA). The timing pulse signals of these stimulations were synchronized to acquire neuronal signals.

In the signal acquisition and processing procedure, signals recorded from the microneedle electrode was differentially amplified (ZC64, Tucker-Davis Technologies, 1 × 10^{14} Ω input impedance) with filters (0.35 Hz for low-cutoff and 7.5 kHz for high-cutoff). Following signal amplification, the signals were routed to a preamplifier/digitizer (PZ2, Tucker-Davis Technologies) and a digital signal processing module (RZ2, Tucker-Davis Technologies, Alachua, USA). All digital data were then stored on a hard disk in a Windows PC with a sampling frequency of 25 kHz.

Immunohistochemistry

Six mice (wild-type C57 BL/6, 20-30 g in weight before implantation) were used for floating and pin-type electrodes, respectively. Each electrode was implanted at the V1 of each

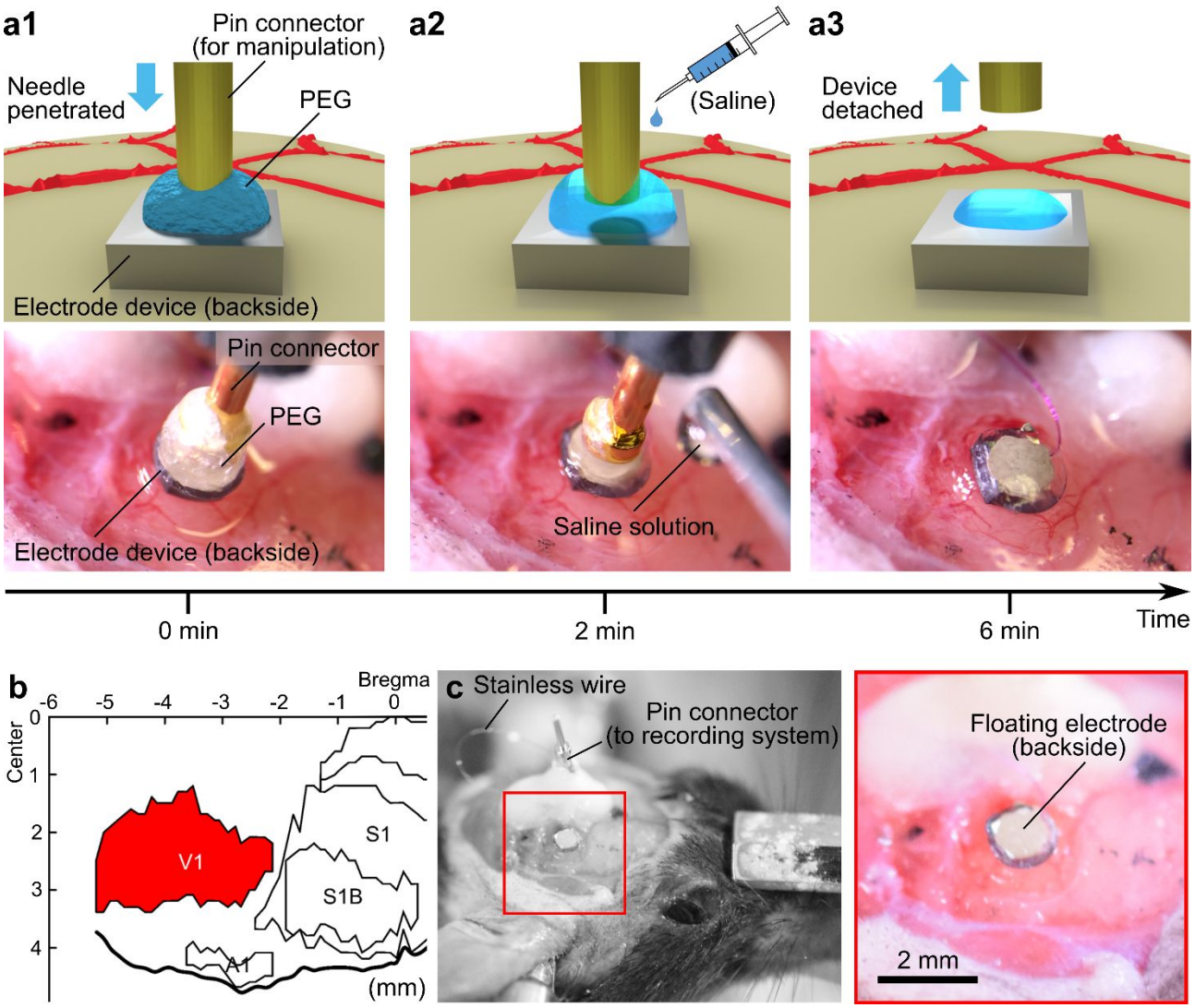

Figure 3. Placement of the floating electrode on the brain tissue of a mouse. a) Schematic and photograph of each step in the surgical procedure for the electrode penetration: a1) the needle electrode penetrates the brain tissue of the mouse by manipulating the pin connector; a2) dropping PBS to the PEG for detaching the electrode's substrate from the pin connector; and a3) pulling the pin connector upward for leaving the electrode device on the tissue. b) Schematic showing the area of the device placement in the cortex (visual cortex, V1). c) Photographs of the electrode device after the surgical method.

mouse's right hemisphere. After 2 weeks of the electrode implantation, these mice were anesthetized by intraperitoneal injection of urethane (200 µl of 10 % solution per 10 g body weight) and then perfusion fixed with 4% paraformaldehyde. Four slice samples (coronal section) from each mouse were prepared. Sections were labeled with GFAP (astrocytes), Iba-1 (microglia), and DAPI (nuclei). Photographs were produced with an Olympus DP74 camera powered by CellSens Dimension software (Version 2.2). The intensities of each cell types were based on outline of each cell generated by edge detection (Find Edges of software ImageJ).

Results

Figure 3 shows the proposed surgical procedure for the electrode placement on the mouse's brain tissue and the device detachment by using a dissolvable material of PEG. The needle electrode penetrated the brain tissue by manipulating the pin connector with a manipulator (Figure 3a1). By dropping solution (PBS) on the PEG, the solid-phase PEG is dissolved (Figure 3a2). After the PEG is completely dissolved, the electrode's substrate can be detached from the pin connector, and the electrode device remains on the surface of the brain tissue (Figure 3a3). The time required in the experimental procedure was within 6 min (Movie S1). Figures 3b and c show an electrode device, which was placed on the V1 on the right hemisphere (2.5 mm on the lateral side and 4.0 mm on the caudal side to the bregma, having a diameter of 1–3 mm). After the device placement, the device was covered with a gelatin sponge and dental cement for the chronic recording (see "In vivo experiments") (Figures 4a and b).

We assessed chronic recording from mice implanted with pin type and floating electrodes (wild-type C57 BL/6, 20-30 g prior to implantation). Figures 4c1 and c2 represent low-frequency (filtering

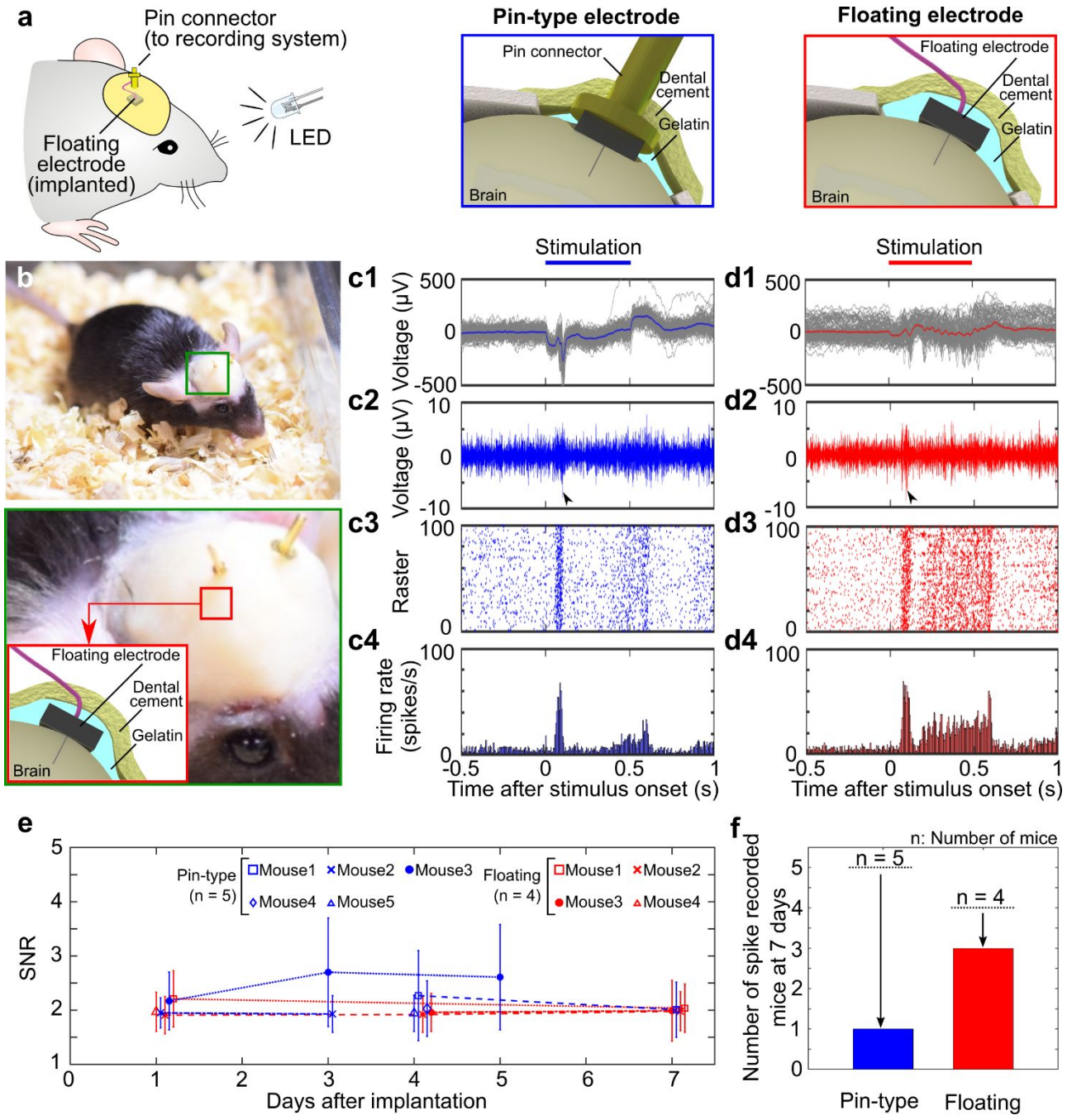

Figure 4. Chronic in vivo neuronal recording for 7 days. a) Schematic of the recording with visual stimulation provided by a light-emitting diode (LED). b) Photographs of a mouse implanted with a floating electrode. To record visual responses, each device is implanted into the mouse's visual cortex (V1). c1–4) Waveforms recorded from the pin-type electrode 1 day after implantation; c1) an average waveform of low-frequency band signals (filtering = 10–80 Hz, n = 100 trials), c2) a single high-frequency band signal from a single trial (filtering = 500–1,000 Hz), and c3, 4) raster plot diagrams and PSTHs extracted from the high-frequency band signals, respectively (n = 100 trials). The detection threshold was set to 3 × the SD (σ) of the mean signal −0.5 to −1.0 s before the stimulus onset. d1–4) Waveforms recorded from the floating electrode 1 day after implantation. e) SNR of spike detected on each electrode implanted mouse for 7 days (mean ± SD, n = 100 trials for each electrode during the recording period). f) Numbers of electrodes detecting spike from each mouse 7 days after implantation.

= 10–80 Hz) and high-frequency (filtering = 500–1,000 Hz) band waveforms, respectively, recorded one day after the pin-type electrode was implanted. Figures 4c3 and c4 show raster plot diagrams and the peristimulus time histograms (PSTHs), respectively, obtained from the high-frequency band signals, with the amplitude threshold of three standard deviations (SDs, σ) of the mean signal −0.5 to −1.0 s before the stimulus onset. Similar to the results obtained with the pin-type electrode, Figures 4d1 and d2 depict waveforms from the low and high-frequency band, respectively, recorded one day after the floating electrode was implanted.

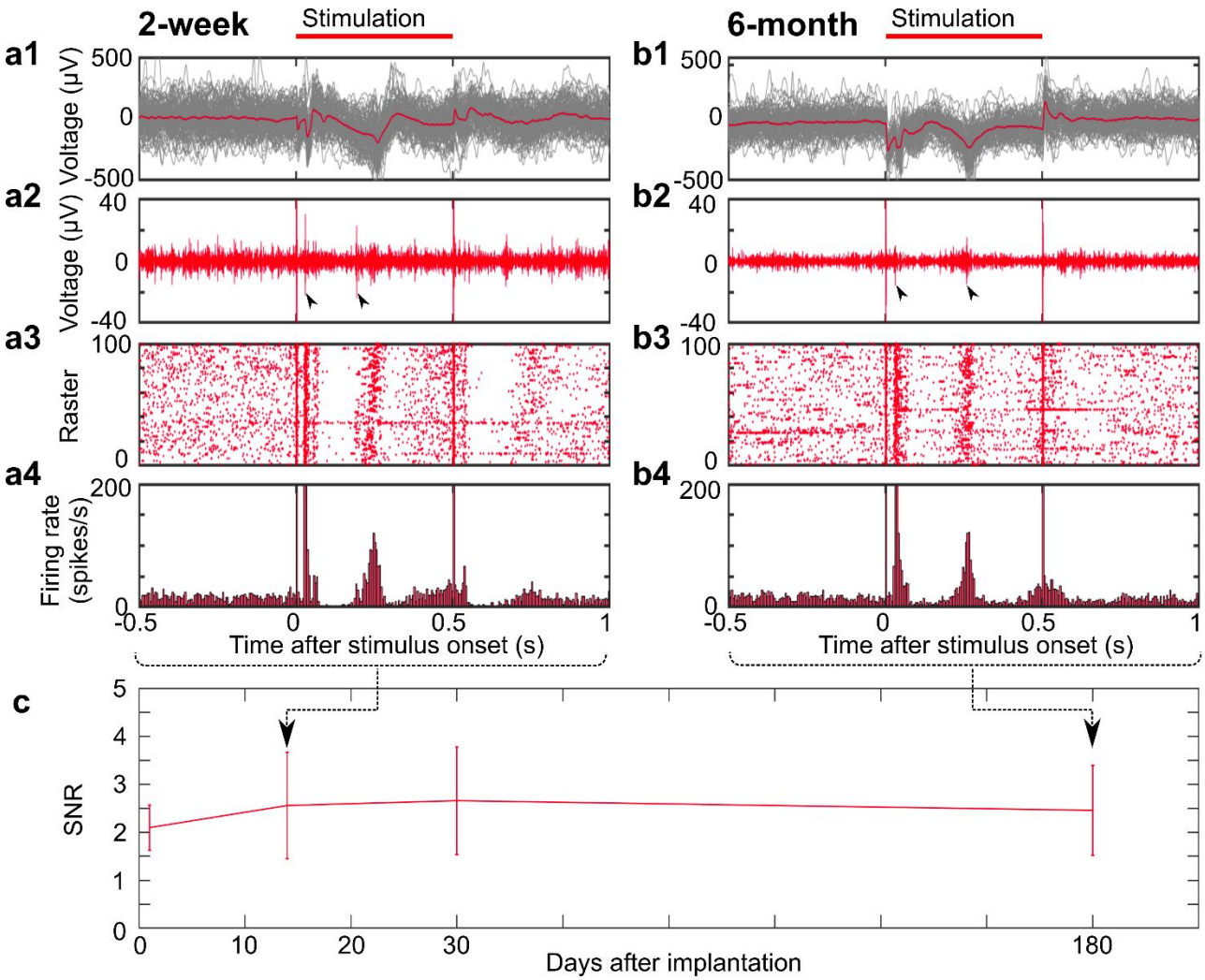

Figure 5. Chronic in vivo neuronal recording with the floating electrode for 6 months. a1–4) Waveforms recorded from the freely moving mouse 2 weeks after the implantation. Top panel represents the timing of the optical stimulation: a1) average waveform of low-frequency band signals (filtering = 10–80 Hz, n = 100 trials), a2) a high-frequency band signal from a single trial (filtering = 500–1,000 Hz), and a3,4) raster plot diagrams and PSTHs taken from the high-frequency signals (n = 100 trials). The detection threshold was 3 × the SD (σ) of the mean signal −0.5 to −1.0 s before the stimulus onset. b1–4) Waveforms recorded from the free-moving mouse 6 months after the implantation. c) SNR of spike detected on the electrode implanted mouse for 180 days (6 months) (mean ± SD, n = 100 trials for each recording period).

Additionally, Figures 4d3 and d4 show raster plot diagrams and the PSTHs detected from the high-frequency band signals using an amplitude threshold (3σ of the mean signal, −0.5 to −1.0 s before the stimulus onset). The signals responding to the visual stimuli appeared at approximately 50 ms, for both pin type and floating electrodes, which was consistent with the latency of mouse's visual response.[29] These results suggest that the recorded signals were subjected to the local field potentials (Figures 4c1 and d1) and the spikes (Figures 4c2–c4 and 4d2–d4), which were evoked by the visual stimuli.

Additionally, we evaluated the chronic recording by comparing the signal-to-noise ratio (SNR) of spikes for a period of 7 days (n = 5 mice for pin-type electrode and n = 4 mice for floating electrode, Figure 4e). The SNR was defined as the peak-to-peak amplitude of the mean waveform 0.005 to 0.1 s after the stimulus onset divided by the 3σ of the noise level. These SNRs are greater than 1.9 (mean) across all electrode types. The duration of the continuous recording on the order land depended not only on the mouse, but also the type of the implanted electrode. The pin-type electrode demonstrated a decrease in the number of electrodes detecting spike signals (3σ of the mean signal −0.5 to −1.0 s before the stimulus onset) from 5 to 1 on day 7. On the other hand, the floating electrode demonstrated a decrease in the number of electrodes from 4 to 3, indicating that it is more stable with the floating electrode than with the pin-type electrode (Figure 4f).

We examined the chronic recording from the floating electrode implanted mouse for a longer period of 6 months (n = 1 mouse, wild-type C57 BL/6, female, 27.8 g in weight before implantation). Figures 5a1, 2 and 5b1, 2 represent low-frequency band (filtering = 10–80 Hz) and high-frequency band (filtering = 500–1,000 Hz) waveforms of the periods of 2 weeks and 6 months, respectively, recorded from the same electrode implanted mouse. Large spikes appeared at 0 and 0.5 s are stimulation–induced artifacts which represent the timing of LED illumination. Figures 5a3, 4 and 5b3, 4 also show raster plot

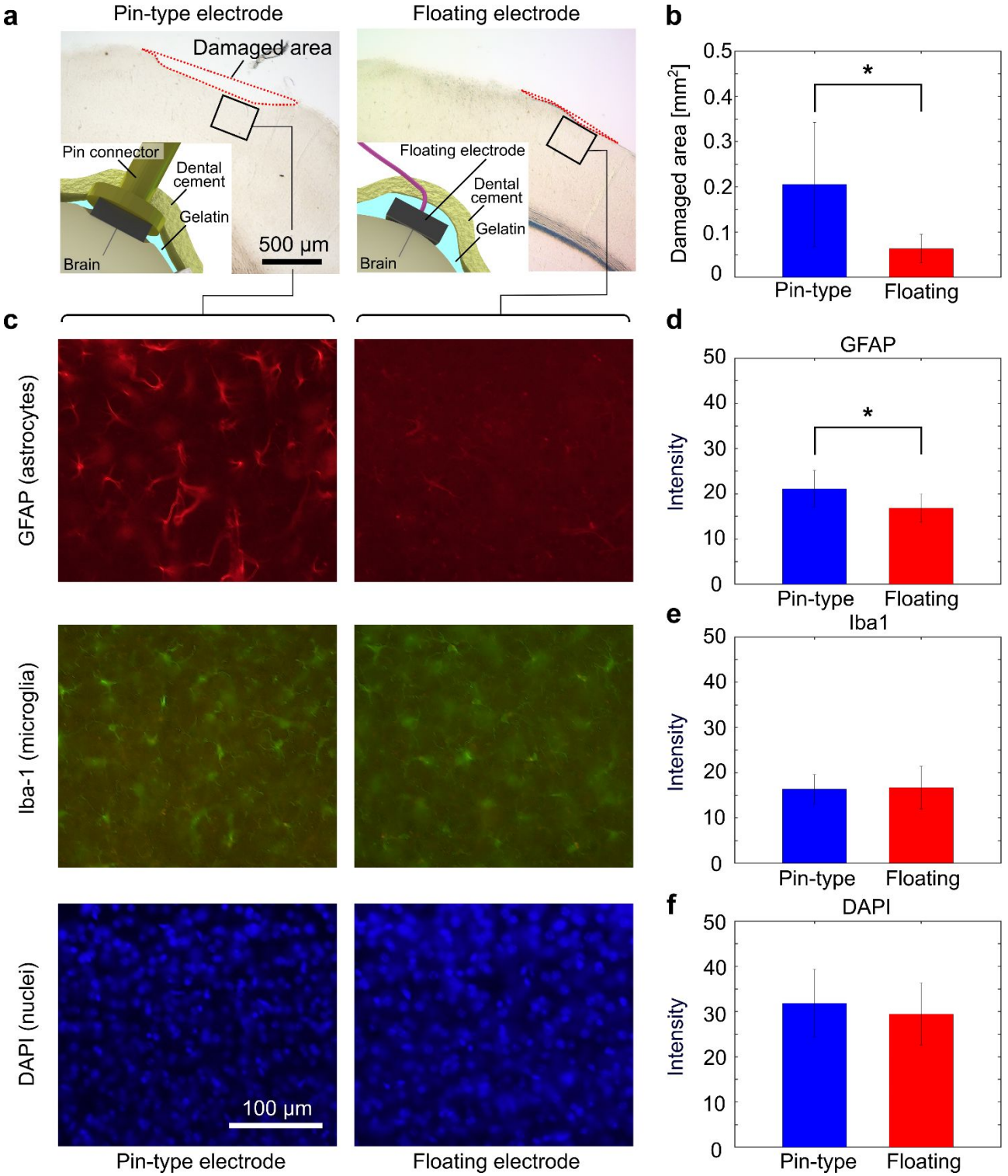

Figure 6. Histological comparison of the tissue response to chronically implanted conventional pin type and floating electrodes. a) Photograph of the brain tissues two weeks after the pin-type electrode and floating electrode were implanted. b) Quantitative comparison of damaged areas on pin type and floating electrodes. c) Tissue responses in the visual cortex following 2-week implantation of a pin-type electrode (left panels) and the floating electrode (right panels). Tissues are labeled for reactive astrocytes (GFAP), microglia (Iba-1), and nuclei (DAPI). d-f) Quantitative comparisons of each cell type between the pin type and floating electrodes using fluorescent intensity in an area of 0.1 mm^2, taken from 24 slices of six mice (mean ± SD) (* $p < 0.01$, t-test).

diagrams and the PSTHs of high-frequency band signals detected at these recording periods (3σ of the mean signal −0.5 to −1.0 s before the stimulus onset). We also analysed the SNR during the recording period (6 months, Figure 5c), showing the mean SNR of > 2.4 from 2 weeks to 6 months without significant degradations.

Additionally, we examined tissue damage associated with the implanted floating device; we also examined tissue damage associated with the pin-type electrode (cranium-fixed electrode) using different mice (n = 3 mice for the floating electrode and n = 3 mice for the pin-type electrode).

Figure 6a shows the brain tissues (coronal section) two weeks after the pin-type electrode and floating device were implanted. Each slice sample shows a dimple-like damaged area at the location of each electrode. Figure 6b shows the quantitative comparison of these damaged areas, which were calculated by smoothing each tissue surface ("damaged area" is depicted in Figure 5a with a red dashed line). The floating electrode significantly reduced the damage area compared to the pin-type electrode (24-slice samples from six mice, t-test, *p < 0.01).

Figure 6c shows the histological outcome (coronal brain section) from the V1 of mice 2 weeks after device implantation, including the distribution of labeled reactive astrocytes (GFAP), microglia (Iba-1), and cell nuclei (DAPI) (24-slice samples from six mice, t-test, *p < 0.01). In comparison to the pin-type electrode, the floating device exhibits fewer reactive astrocytes (Figure 6d). The microglia (Iba-1) and cell nuclei (DAPI) associated with the floating electrode were compared to those of the pin-type electrode (Figures 6e and f), and no statistically significant difference was observed. These histological findings indicate that the floating device is capable of recording for extended period of time while minimizing tissue responses, compared to the pin-type.

Discussion

We proposed the penetration of a microelectrode into the brain tissue and the device detachment with dissolvable material of PEG. The advantage of the proposed surgical procedure is the reduction of the physical stress to the tissue during the device placement as well as the detachment from the manipulator.[10] Other material of paraffin wax was also used in our prior work[27] ; however, this material needed to be heated for melting (~70℃), while the used PEG dissolves with PBS at room temperature. The time required for the device placement was ~10 min, a period that can be adjusted by changing the molecular weight of the PEG used. As an advanced way to use the dissolvable material, we can use a PEG-containing bioactive agent, which would reduce immune responses of the tissue.[30]

For a period of 7 days following implantation, neuronal recordings were demonstrated using the pin type and proposed floating electrodes implanted in mice. Throughout the recording period, the number of pin electrodes detecting spike signals decreased from 5 to 1, while the number of floating electrodes decreased from 4 to 3 (Figure 4f). The SNR varied between recordings (date and mouse), indicating that there was no significant difference between these two types of electrodes, whereas the recording duration (days) was dependent on the mice. Additionally, we confirmed that some mice did not exhibit spike recording in the early days (1–3 days post implantation); however, these mice displayed spike recording in later days (e.g., 3–7 days post implantation). The temporal loss of spike signals was almost certainly caused by the initial impact of the needle penetration, which compresses and slashes tissue as well as early responses (e.g., activated microglia[13]). This indicates that the initial impact is independent of the electrode type (pin type and floating). Additionally, the result of recovered spike recording with the floating electrode in later days (e.g., 3–7 days post implantation) indicates that the floating electrode contributes to the reduction of inflammation caused by micromotion[31,32] between the electrode and brain tissue.

We also analyzed the SNR during the floating electrode implanted mouse for 6 months. As known, the implanted device fixed to the cranium induces the motion of the needle in the tissue, resulting in continuous repeated injury to the brain tissue.[11,33,34] This continuous injury forms glial scars, which act as an electrical insulating layer around the recording site of the needle electrode. However, the SNRs measured from 2 weeks to 6 months showed no significant degradation. These results suggest that the floating electrode enables following the tissue motion and reduces the continuous injury.

We examined tissue damage associated with the proposed floating electrode and pin-type electrode. The result indicated that the floating device shows a dimple-like damaged area four times smaller than the damaged area of the pin-type electrode. This result suggested that the device substrate of the pin-type electrode, which is fixed to the cranium, induced pressure to the brain surface during the device implantation. It is known that pressure to the brain tissue causes cerebral ischemia, which results in a blood-brain barrier breach as well as biological inflammation.[35,36] Alternatively, the floating electrode showed a smaller damaged area in the tissue (Figures 6a and b), which could minimize the issues associated with the electrode implantation.

For the further quantitative comparison of reactive astrocytes (GFAP, Figure 6d), we confirmed these fewer astrocytes with the floating electrode. This result represents the effect of the floating electrode, which was not fixed to the cranium to enable following the tissue. However, comparisons of other cell types of microglia (Iba-1, Figure 6e) and nuclei (DAPI, Figure 6f) showed no significant differences between the floating and pin-type electrodes. These phenomena were due to the observation period of 2 weeks, in which microglia formed in response to the injury (over hours and days[34]) and astrocytes became activated afterwards (for 2 weeks and beyond[13]). Although the floating electrode showed these less tissue damage than did the pin-type electrode, further minimized tissue damage will be required for future implantation.

For the recording of neuronal activities from the mouse's cortex, we used a single-channel electrode with a 5-µm-diameter microneedle and a device size of 1 × 1 mm^2 to record neuronal activity from the mouse cortex. While the floating technique minimized tissue damage (Figure 6), the device's dimensions are insufficient for the application of multisite recording with these devices. By arranging these electrode devices, however, a craniotomy area larger than that of a single-channel electrode (>1–3 mm diameter, Figure 3c) will be required. This indicates that the size of these arranged devices is not small enough for particular brain areas in the mouse (e.g., 2 × 3 mm^2 in primary visual cortex [V1]). Therefore, we are currently working on fabricating even smaller devices (<1 × 1 mm^2) using the same fabrication process that used in this

work.[20] These results of device miniaturization and multisite recording will be reported in a future publication.

In addition, the floating electrode device presented here includes an additional cable that connects the mouse (electrode device) to the first-stage amplifier of the recording system. This cable may result in inhabitation of the mouse's behavior as well as a decrease in the recording signal quality due to external noise coupled with the cable. These concerns can be resolved with a wireless electrode recording system.[37–41]

Conclusions

In summary, we proposed a method for chronic neuronal recording in mice in which a 5-µm-diameter microneedle electrode penetrates brain tissue via dissolvable material-based detachment and remains on it without being fixed to the cranium, resulting in a floating electrode architecture. Although the electrode device requires further advancements such as miniaturization and wireless recording system, the proposed recording technology showed clear advantages in terms of the high SNR during implantation and less tissue damage. These findings show that the proposed method will enable stable and safe chronic recording in not only the mice demonstrated in this study but also other animals, including rats and monkeys.

Author Contributions

K. Y., H. S., and T. K. designed the research. S. Ya. and K. Y. prepared devices. K. Y. conducted surgical procedure, animal experiment, immunohistochemical experiment. K. Y., R. N., K. K., and T. K. analyzed data. S. Yo. helped the immunohistochemical experiment. K. Y. and T. K. wrote the manuscript. T. K. supervised the project.

Conflicts of interest

There are no conflicts to declare.

Acknowledgements

We acknowledge support from JSPS KAKENHI Grant Numbers 17H03250, 26709024, and 20H00244, for the Strategic Advancement of Multi-Purpose Ultra-Human Robot and Artificial Intelligence Technologies program from NEDO, Adaptable and Seamless Technology transfer Program through Target-driven R&D (A-STEP) from JST, and Nagai Foundation for Science & Technology. R. N. was supported by Takeda Science Foundation. K. K. was supported by JSPS KAKENHI Grant Number 15H05917, 20H00614.

Notes and references

1 P. J. Rousche and R. A. Normann, *Journal of Neuroscience Methods*, 1998, **82**, 1–15.

2 Q. Bai, K. D. Wise and D. J. Anderson, *IEEE Transactions on Biomedical Engineering*, 2000, **47**, 281–289.

3 J. J. Jun, N. A. Steinmetz, J. H. Siegle, D. J. Denman, M. Bauza, B. Barbarits, A. K. Lee, C. A. Anastassiou, A. Andrei, Ç. Aydin, M. Barbic, T. J. Blanche, V. Bonin, J. Couto, B. Dutta, S. L. Gratiy, D. A. Gutnisky, M. Häusser, B. Karsh, P. Ledochowitsch, C. M. Lopez, C. Mitelut, S. Musa, M. Okun, M. Pachitariu, J. Putzeys, P. D. Rich, C. Rossant, W. L. Sun, K. Svoboda, M. Carandini, K. D. Harris, C. Koch, J. O'Keefe and T. D. Harris, *Nature*, 2017, **551**, 232–236.

4 A. Obaid, M.-E. Hanna, Y.-W. Wu, M. Kollo, R. Racz, M. R. Angle, J. Müller, N. Brackbill, W. Wray and F. Franke, *Science advances*, 2020, **6**, eaay2789.

5 S. Takeuchi, T. Suzuki, K. Mabuchi and H. Fujita, *Journal of micromechanics and microengineering*, 2003, **14**, 104.

6 T. il Kim, J. G. McCall, Y. H. Jung, X. Huang, E. R. Siuda, Y. Li, J. Song, Y. M. Song, H. A. Pao, R. H. Kim, C. Lu, S. D. Lee, I. S. Song, G. Shin, R. Al-Hasani, S. Kim, M. P. Tan, Y. Huang, F. G. Omenetto, J. A. Rogers and M. R. Bruchas, *Science*, 2013, **340**, 211–216.

7 B. J. Kim, J. T. W. Kuo, S. A. Hara, C. D. Lee, L. Yu, C. A. Gutierrez, T. Q. Hoang, V. Pikov and E. Meng, *Journal of neural engineering*, 2013, **10**, 045002.

8 L. Luan, X. Wei, Z. Zhao, J. J. Siegel, O. Potnis, C. A. Tuppen, S. Lin, S. Kazmi, R. A. Fowler, S. Holloway, A. K. Dunn, R. A. Chitwood and C. Xie, *Science Advances*, 2017, **3**, 1–10.

9 E. Musk, *Journal of medical Internet research*, 2019, **21**, e16194.

10 K. Yamashita, H. Sawahata, S. Yamagiwa, Y. Morikawa, R. Numano, K. Koida and T. Kawano, *Sensors and Actuators B: Chemical*, 2020, **316**, 127835.

11 R. Biran, D. C. Martin and P. A. Tresco, *Experimental Neurology*, 2005, **195**, 115–126.

12 V. S. Polikov, P. A. Tresco and W. M. Reichert, *Journal of Neuroscience Methods*, 2005, **148**, 1–18.

13 H. Szarowski, D. Andersen, S. Retterer, J. Spence, M. Isaacson, G. Craighead, N. Turner and W. Shain, *Brain Research*, 2003, **983**, 23–35.

14 R. Chen, A. Canales and P. Anikeeva, *Nature Reviews Materials*, 2017, **2**, 1–16.

15 S. M. Wellman, K. Guzman, K. C. Stieger, L. E. Brink, S. Sridhar, M. T. Dubaniewicz, L. Li, F. Cambi and T. D. Y. Kozai, *Biomaterials*, 2020, **239**, 119842.

16 T. D. Y. Kozai, X. Li, L. M. Bodily, E. M. Caparosa, G. A. Zenonos, D. L. Carlisle, R. M. Friedlander and X. T. Cui, *Biomaterials*, 2014, **35**, 9620–9634.

17 A. Hai, J. Shappir and M. E. Spira, *Nature methods*, 2010, **7**, 200–202.

18 L. Grob, H. Yamamoto, S. Zips, P. Rinklin, A. Hirano-Iwata and B. Wolfrum, *Advanced Materials Technologies*, 2020, **5**, 1900517.

19 T. D. Y. Kozai, N. B. Langhals, P. R. Patel, X. Deng, H. Zhang, K. L. Smith, J. Lahann, N. A. Kotov and D. R. Kipke, *Nature materials*, 2012, **11**, 1065.

20 H. Sawahata, S. Yamagiwa, A. Moriya, T. Dong, H. Oi, Y. Ando, R. Numano, M. Ishida, K. Koida and T. Kawano, *Scientific Reports*, 2016, **6**, 35806.

21 A. Fujishiro, H. Kaneko, T. Kawashima, M. Ishida and T. Kawano, *Scientific Reports*, 2014, **4**, 1–9.

22 Y. Kubota, S. Yamagiwa, H. Sawahata and S. Idogawa, *Sensors & Actuators: B. Chemical*, 2018, **258**, 1287–1294.

23 D. Seo, R. M. Neely, K. Shen, U. Singhal, E. Alon, J. M. Rabaey, J. M. Carmena and M. M. Maharbiz, *Neuron*, 2016, **91**, 529–539.

24 B. C. Johnson, K. Shen, D. Piech, M. M. Ghanbari, K. Y. Li, R. Neely, J. M. Carmena, M. M. Maharbiz and R. Muller, in *2018 IEEE Custom Integrated Circuits Conference (CICC)*, IEEE, 2018, pp. 1–4.

25 S. Yamagiwa, H. Sawahata, H. Oi, R. Numano, M. Ishida, K. Koida and T. Kawano, in *2017 IEEE 30th International Conference on Micro Electro Mechanical Systems (MEMS)*, IEEE, 2017, pp. 553–556.

26 A. Ikedo, T. Kawashima, T. Kawano and M. Ishida, *Applied Physics Letters*, 2009, **95**, 33502.

27 K. Yamashita, H. Sawahata, S. Yamagiwa, R. Numano, K. Koida and T. Kawano, in *2019 20th International Conference on Solid-State Sensors, Actuators and Microsystems & Eurosensors XXXIII (TRANSDUCERS & EUROSENSORS XXXIII)*, IEEE, 2019, pp. 302–305.

28 H. Oka, K. Shimono, R. Ogawa, H. Sugihara and M. Taketani, 1999, **93**, 61–67.

29 K. Funayama, N. Hagura, H. Ban and Y. Ikegaya, *Journal of Neuroscience*, 2016, **36**, 11727–11738.

30 A. Lecomte, V. Castagnola, E. Descamps, L. Dahan, M. C. Blatché, T. M. Dinis, E. Leclerc, C. Egles and C. Bergaud, *Journal of Micromechanics and Microengineering*, , DOI:10.1088/0960-1317/25/12/125003.

31 J. C. Barrese, N. Rao, K. Paroo, C. Triebwasser, C. Vargas-Irwin, L. Franquemont and J. P. Donoghue, *Journal of neural engineering*, 2013, **10**, 066014.

32 G. Lind, C. E. Linsmeier and J. Schouenborg, *Scientific reports*, 2013, **3**, 1–7.

33 N. J. Michelson, A. L. Vazquez, J. R. Eles, J. W. Salatino, E. K. Purcell, J. J. Williams, X. T. Cui and T. D. Y. Kozai, *Journal of neural engineering*, 2018, **15**, 33001.

34 T. D. Y. Kozai, A. L. Vazquez, C. L. Weaver, S.-G. Kim and X. T. Cui, *Journal of neural engineering*, 2012, **9**, 66001.

35 S. Zhang, J. Boyd, K. Delaney and T. H. Murphy, *Journal of Neuroscience*, 2005, **25**, 5333–5338.

36 S. M. Wellman, L. Li, Y. Yaxiaer, I. McNamara and T. D. Y. Kozai, *Frontiers in neuroscience*, 2019, **13**, 493.

37 D. Fan, D. Rich, T. Holtzman, P. Ruther, J. W. Dalley, A. Lopez, M. A. Rossi, J. W. Barter, D. Salas-Meza and S. Herwik, *PloS one*, 2011, **6**, e22033.

38 T. A. Szuts, V. Fadeyev, S. Kachiguine, A. Sher, M. v Grivich, M. Agrochão, P. Hottowy, W. Dabrowski, E. v Lubenov and A. G. Siapas, *Nature neuroscience*, 2011, **14**, 263–269.

39 A. Zhou, S. R. Santacruz, B. C. Johnson, G. Alexandrov, A. Moin, F. L. Burghardt, J. M. Rabaey, J. M. Carmena and R. Muller, *Nature biomedical engineering*, 2019, **3**, 15–26.

40 M. H. Ghaed, G. Chen, R. Haque, M. Wieckowski, Y. Kim, G. Kim, Y. Lee, I. Lee, D. Fick and D. Kim, *IEEE Transactions on Circuits and Systems I: Regular Papers*, 2013, **60**, 3152–3162.

41 S. Idogawa, K. Yamashita, R. Sanda, R. Numano, K. Koida and T. Kawano, *Sensors and Actuators B: Chemical*, 2021, **331**, 129423.